Downloaded from orbit.dtu.dk on: May 05, 2023

DTU Library

Optimizing Synthetic Aperture Compound Imaging

Hansen, Jens Munk; Jensen, Jørgen Arendt

Published in:
Proceedings of IEEE International Ultrasonics Symposium. IEEE, 2012

Publication date:
2012

Document Version
Early version, also known as pre-print

Link back to DTU Orbit

Citation (APA):
Hansen, J. M., & Jensen, J. A. (2012). Optimizing Synthetic Aperture Compound Imaging. In *Proceedings of IEEE International Ultrasonics Symposium. IEEE, 2012* IEEE.

General rights
Copyright and moral rights for the publications made accessible in the public portal are retained by the authors and/or other copyright owners and it is a condition of accessing publications that users recognise and abide by the legal requirements associated with these rights.

- Users may download and print one copy of any publication from the public portal for the purpose of private study or research.
- You may not further distribute the material or use it for any profit-making activity or commercial gain
- You may freely distribute the URL identifying the publication in the public portal

If you believe that this document breaches copyright please contact us providing details, and we will remove access to the work immediately and investigate your claim.

Optimizing Synthetic Aperture Compound Imaging

Jens Munk Hansen[†⋆] and Jørgen Arendt Jensen[†].
[†]Center for Fast Ultrasound Imaging, Dept. of Elec. Eng,
Technical University of Denmark, DK-2800 Lyngby, Denmark
⋆ BK-Medical,
Mileparken 34, DK-2730 Herlev, Denmark

***Abstract*—Spatial compound images are constructed from synthetic aperture data acquired using a linear phased-array transducer. Compound images of wires, tissue, and cysts are created using a method, which allows both transmit and receive compounding without any loss in temporal resolution. Similarly to conventional imaging, the speckle reduction achieved by spatial compounding comes at the cost of a reduced detail resolution and a compromise must be made. Using a performance indicator, which can be measured from an image of a phantom without cysts, it is demonstrated how a compromise can be made, which is optimal for lesion detection. Synthetic aperture data are acquired from unfocused emissions and 154 compound images are constructed by synthesizing different aperture configurations with more or less compounding, all maintaining a constant resolution across depth corresponding to an f-number of 2.0 for transmit and receive. The same configurations are used for scanning a phantom with cysts, and it is demonstrated how an improved cysts contrast follows from an aperture configuration, which gives a higher value for the performance measure extracted from the phantom without cysts. A correlation value $R = 0.81$ is observed with a p-value less than 0.0001. For the optimal compound image, the contrast is improved by 3 dB for a cyst at a depth of 50 mm compared to an image without compounding.**

I. Introduction

Ultrasound imaging is subject to a number of inherent artifacts that compromise image quality. The most prominent artifact is the degradation by *speckle*, which reduces image contrast, and diminishes the possibilities for detection of low-contrast regions [1], [2]. One of the most successful approaches for removing speckle is spatial compounding, where the speckle is reduced by averaging decorrelated frames [3], [4]. A major drawback of spatial compounding is that speckle reduction comes at a cost of a reduction in frame rate by the number of directions used for compounding. Using synthetic aperture data, compounding can be achieved using any number of directions without reducing the frame rate as shown in [5].

Another challenge with spatial compounding is that speckle reduction comes at the cost of a reduced detail resolution and a compromise between contrast and resolution must always be made. This compromise was first studied by Burckhardt [1], who computed the theoretical value for the contrast or more precisely, the number of independent images, N_{eff}. This number can be computed by studying the correlation function between pulse-echo measurements at different spatial positions. In particularly, he demonstrated, how compounding by translating the aperture by half it length, results in at most 2.25 independent images per aperture. In later publications, Wagner et al. [6] have shown through theoretical considerations, and Trahey et al. [4] through measurements that the approximate form for the correlation function presented by Burckhardt is inaccurate in the sense that it overestimates the correlation. The measurements by Trahey et al. show that translating the aperture by half its length, results in about 3.2 independent images per aperture and even closer spacing allows more effective compounding. O' Donnell and Silverstein derived an exact analytic expression for the pulse-echo correlation function [7], and it is now well known that the conclusions made by Burckhardt are inaccurate.

The analytic expression matches the measurements of Trahey et al. reasonably well and can be used for deriving the optimum aperture displacement for efficient compounding to be about half the aperture length, when using three apertures and smaller when using more compound apertures.

With the possibility for real-time synthetic aperture imaging [8], [9], [10] and compounding without compromising the frame rate [5], new attention should be given to optimizing images using spatial compounding. In particularly, since the expression made by O' Donnell and Silverstein is derived by assuming both transmit and receive focusing, which is attained by synthetic aperture focusing. Inspired by their work, this paper investigates through measurements, how synthetic aperture compound images can be optimized using a figure of merit for the task of lesion detection. In addition, it suggests another performance indicator, which can be extracted from a tissue-mimicking phantom without cysts and by studying different aperture configurations with more or less compounding, an optimal compound configuration can be found for lesion detection.

II. Synthetic Aperture Compound Imaging

To perform spatial compounding using synthetic aperture data, the linearity of delay-and-sum beamformation is exploited to synthesize multiple transmit and receive apertures using data from part of or all of a number of unfocused emissions [11], [12], [13]. For each point in the image, beam apodization values are calculated corresponding to insonifying the point using focused beams from a number, N_{s}, of synthetic apertures with different locations. In Fig. 1, it is shown for a single point, $\vec{r}_{\text{fp}}$, how the beam apodization for an emission with origin $\vec{r}_{\text{xmt}}$ is calculated using the distance from the transmit origin, $\vec{r}_{\text{xmt}}$ to the scan line - the line connecting the point, $\vec{r}_{\text{fp}}$ with the center of a synthetic aperture, the aperture

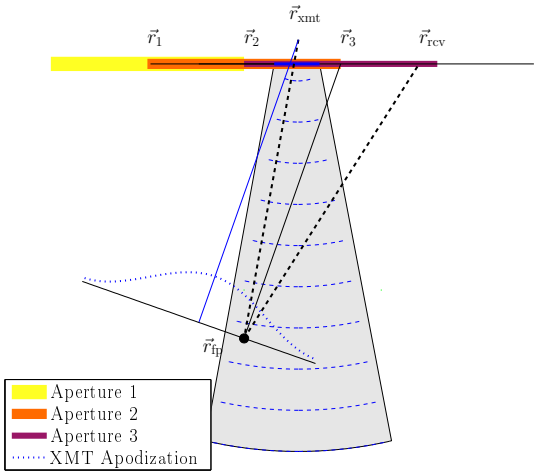

Figure 1. Beam apodization calculation for a single image point $\vec{r}_{\mathrm{fp}}$ for a sub-image using an aperture located at $\vec{r}_3$, Aperture 3. The apodization values can be read-off the figure as the intersection of the scan line and the apodization profiles. The shaded region is the region insonified by the active elements used for the unfocused emission with origin $\vec{r}_{\mathrm{xmt}}$.

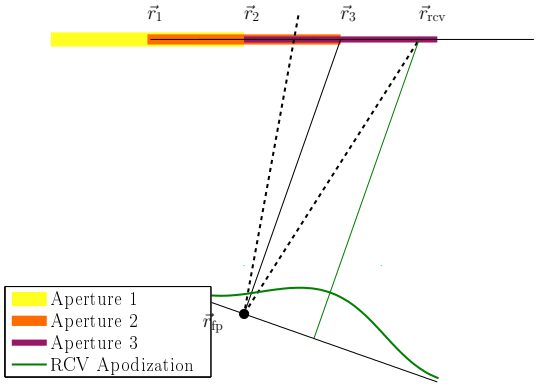

Figure 2. Receive apodization calculation for a single image point $\vec{r}_{\mathrm{fp}}$ for a sub-image using an aperture located at $\vec{r}_3$, Aperture 3. The apodization values can be read-off the figure as the intersection of the scan line and the apodization profiles.

located at $\vec{r}_3$. Similarly, receive apodizations are calculated for each point and applied to the signals received from the individual receiving elements of each transmission. The receive apodization values are calculated using the distance from the scan line to the position of the receiving elements as shown in Fig. 2. For the setup used in this paper, the apertures are selected such that they overlap equally and are distributed symmetrically around the image point. The situation shown in Fig. 1 and Fig. 2 apply to a setup with three apertures, $N_{\mathrm{s}} = 3$ and where they overlap by 50%. For each emission, this procedure is repeated for a range of subapertures $i = 1, \ldots N_{\mathrm{s}}$ to update N_{s} images used for compounding. To avoid the need for sampling according to the Nyquist criterion for the excitations used in all the directions of the scan lines, the RF data are beamformed as in-phase and quadrature components, and the envelope for each angular image is simply computed as the absolute value [14]. Finally, the compound image are constructed by adding the enveloped images.

A. *Figure of merit*

The figure of merit referred to in the introduction was introduced by Smith. et al. and later used by O' Donnell and Silverstein for computing the optimum aperture displacement for efficient compounding [7]. It is given by [15]

$$f_{\mathrm{m}} = N_{\mathrm{eff}} L_{\mathrm{s}} / L, \tag{1}$$

where L and L_{s} are, respectively the length of the aperture and the length of the subaperture(s) used for compounding. The fractional size of the subaperture, L_{s}/L is a measure for the lateral resolution of the imaging system and N_{eff} is a measure for the efficiency of compounding. By qualifying images using the product (1), a compound image made by adding two independent measurements is as good as an image with twice the lateral resolution. It should be noted that this measure is a measure for detecting intensity differences between a region of interest (ROI) and its surroundings. In Fig. 5a, multiple values for N_{eff} are computed and the product (1) is shown for a range of compound configurations. The abscissa, x represents the relative displacement of the apertures used for compounding. From Fig. 5a it follows that the product (1) peaks for configurations, where the apertures are displaced with about half their length.

To verify the theoretical value for the figure of merit using measurements, the number of independent images, N_{eff} can be estimated by measuring the correlation between the sub-images or by measuring the signal-to-noise ratio at a point SNR_0 and using that the enveloped signals follow Rayleigh statistics [2]

$$N_{\mathrm{eff}} = \left(\frac{\mathrm{SNR}_0}{1.91} \right)^2. \tag{2}$$

The signal-to-noise ratio at a point, SNR_0 is defined as

$$\mathrm{SNR}_0 \equiv \frac{\mu_V}{\sigma_V},$$

where μ_V and σ_V are the expectation value and standard deviation of the envelope-detected signals.

B. *Speckle information density*

The figure of merit defined in the last section can be used as rule of thumb for how spatial compounding should be implemented. However, for assessing the quality of an image, it is not sufficient to measure the mean and standard deviation of a region in a tissue image and computing the figure of merit. The reason is that it doesn't capture the resolution and further improper focusing leads to blurring, which causes N_{eff} to increase and too high a value for the figure of merit is obtained. The most obvious solution is to measure the detail resolution using a wire phantom and replace the size of the subaperture(s), L_{s} in (1) with the size of an effective aperture, $\tilde{L}_{\mathrm{s}}$ derived from the full width at half maximum of the point spread function

$$\mathrm{FWHM} \simeq 1.22\, \lambda \frac{D}{\tilde{L}_{\mathrm{s}}}. \tag{3}$$

Table I
COMPOUND APERTURE CONFIGURATIONS. N IS THE NUMBER OF SUBAPERTURES, x IS THE RELATIVE APERTURE DISPLACEMENT, AND L_s/L IS THE FRACTIONAL SIZE OF THE SUBAPERTURE(S).

	x	N	L_s/L	Symbol
SA	-	1	1.00	$\bullet$
SAC_2	0.20	2	0.83	$*$
SAC_3	0.25	3	0.67	$+$

In (3), D is the depth and λ is the wave-length of the pulse. In addition to measure the resolution and speckle reduction, it would also be of interest to measure the object contrast, which can be measured using the contrast-to-noise ratio (CNR)

$$\mathrm{CNR} = \frac{|\mu_{I_{\mathrm{ROI}}} - \mu_{I_{\mathrm{B}}}|}{\sqrt{\sigma^2_{I_{\mathrm{ROI}}} + \sigma^2_{I_{\mathrm{B}}}}} = \frac{\Delta I}{\sqrt{\sigma^2_{I_{\mathrm{ROI}}} + \sigma^2_{I_{\mathrm{B}}}}}, \tag{4}$$

where $\mu_{I_{\mathrm{ROI}}}$ and $\mu_{I_{\mathrm{B}}}$ are the mean intensities of the ROI and background, and $\sigma^2_{I_{\mathrm{ROI}}}$ and $\sigma^2_{I_{\mathrm{B}}}$ are their corresponding variances. Instead of imaging a wire-phantom, a speckle phantom, and using some calibrated cyst phantoms for assessing the contrast, we suggest that the *speckle information density* is measured, which can be obtained solely by scanning a tissue phantom without cysts. The speckle information density is derived from a signal-to-noise ratio associated with lesion detection introduced [15]

$$\mathrm{SNR}_{\Delta I} = \frac{C d {N_{\mathrm{eff}}}^{1/2}}{(S_{\mathrm{lat}} S_{\mathrm{ax}})^{1/2}}, \tag{5}$$

where C is the contrast of a circular lesion of diameter d, N_{eff} is the number of independent images compounded, and S_{lat}, and S_{ax}, are the lateral and axial speckle dimension. For a measurement situation, the only ingredient we can optimize in (5) is N_{eff} and the speckle dimensions. It is therefore natural to define the speckle information as $\mathrm{SID} = N_{\mathrm{eff}}/(S_{\mathrm{lat}} S_{\mathrm{ax}})$. The speckle dimensions, S_{lat} and S_{ax} can be found from the correlation cell [16]

$$S_c = \int_{-\infty}^{\infty} \frac{C_I(\Delta\xi)}{C_I(0)} d(\Delta\xi), \tag{6}$$

where C_I is the spatial auto-covariance for the intensity and $\Delta\xi$ is the distance between image pixels.

III. RESULTS

Images of wires, tissue, and cysts were created using a 3.5 MHz phased array transducer with 128 elements. The sampling was done at 35 MHz using the research scanner SARUS [17]. A 16-element subaperture was used for 128 unfocused emissions with an f-number of -0.5. Images were created using 154 different aperture configurations by varying L_s and the relative aperture displacement, x, for $N_s = 1, \ldots, 10$ subapertures.

A. Wire phantom measurements

In Fig. 3, three wire phantom images are shown. The images are created using the aperture configuration listed in Table I. It follows from Fig. 3b and Fig. 3c that by compounding smaller and smaller apertures, the resolution is progressively degraded.

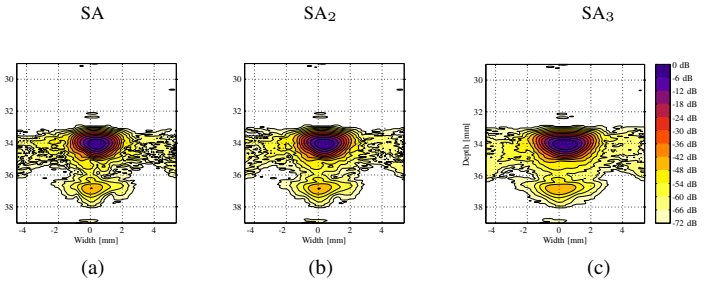

Figure 3. Wire phantom images using the aperture configurations listed in Table I.

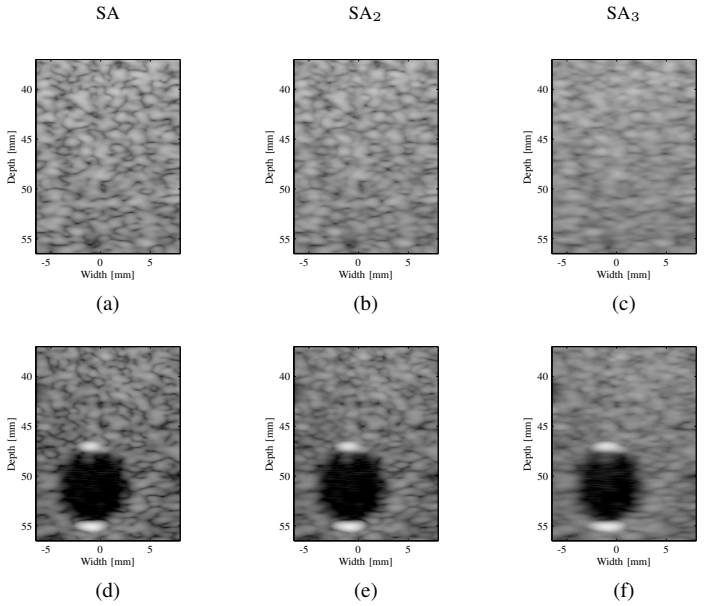

Figure 4. Speckle and cyst images created using the aperture configurations listed in Table I.

B. Tissue and cyst phantom measurements

Using the same aperture configurations, which was used for scanning the wire phantom, tissue and cyst images were created. In Fig. 4, the images are shown.

C. Method validation

It should be clear from the previous sections that synthetic aperture compounding indeed reduces the appearance of speckle at the cost of a reduced detail resolution. The interesting question is now, which aperture configuration is the most optimal for lesion detection or in other words, how much compounding should be introduced. In Fig. 5b, 154 aperture configuration are used for imaging a region of speckle and the values for N_{eff} are extracted and the figure of merit is computed for each configuration. The images used for the 3 configurations marked with $\bullet$, $*$, and $+$ are the 3 tissue images shown in Fig. 4. Comparing the results with the theoretical results in Fig. 5a, a clear correspondence is seen. From the measurement results in Fig. 5b, it follows that the optimal configurations are shifted towards smaller translations of the apertures, which corresponds to larger overlap. This

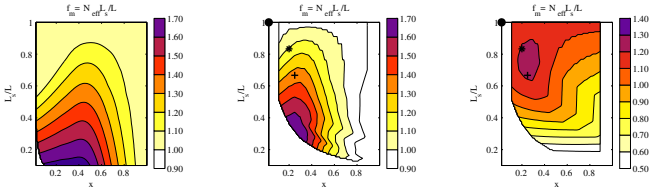

(a) Theory (b) Fixed aperture (c) f = 2.00

Figure 5. Figure of merit computed theoretically and from measurement results.

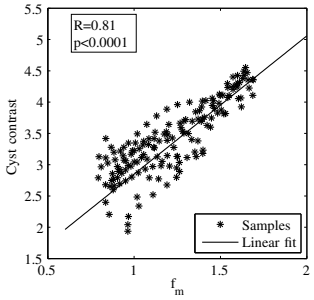

Figure 6. Correlation of CNR values obtained for the cyst at the depth of 50 mm and the figure of merit computed from the speckle images.

can be explained by the fact that a Hamming apodization was introduced when computing the beam and line apodizations for the measurements and the theoretical results are based on an rectangular aperture function. Also, it can be seen that the results are shifted towards using larger subapertures, which is due to the same reason. In Fig. 6, 154 different aperture configurations are used for imaging speckle and the cyst at 50 mm. The values for the figure of merit and the CNR values are correlated against each other and a linear fit is applied to the results. It follows that a large CNR value follows from a configuration, which yields a large value for the figure of merit. The images used for the analysis were created as proposed by the theory and therefore they have different detail resolution. In Fig. 5c, 154 aperture configurations are used, where the apertures are positioned equally to those used for creating Fig. 5b, but in addition the apertures are scaled to maintain a constant f-number of 2.0. Very interesting, the analysis reveals that the configuration giving the largest value for the figure of merit is a configuration with apertures of size equal to about 80% of the full array and displaced about 20%.

In Fig. 6, the speckle information density and the CNR values are computed for the 3 configurations listed in Table I. The cyst and speckle images used are the images shown in Fig. 4. The results show that also the speckle information density is increased for a configuration with improved contrast, but a more thorough study needs to be performed for making a solid statement.

IV. Conclusion

Synthetic aperture compound images were created with success and a simple way for selecting an optimal aperture

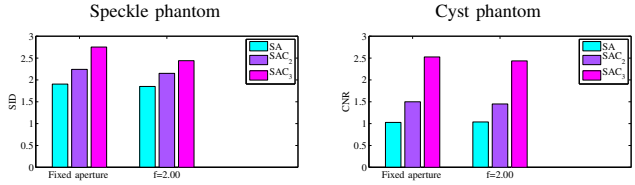

Figure 7. CNR values and SID values for the 3 configurations listed in Table I.

configuration was presented. Whether or not the speckle information density can be used as a standalone performance measure for lesion detection is still unclear, but this area definitely deserves more attention, when synthetic aperture compounding is used for imaging.

References

[1] C. Burckhardt, "Speckle in ultrasound b-mode scans," *IEEE Trans. Son. Ultrason.*, vol. SU-25, no. 1, pp. 1–6, Jan. 1978.

[2] R. F. Wagner, S. W. Smith, J. M. Sandrick, and H. Lopez, "Statistics of speckle in ultrasound B-scans," *IEEE Trans. Son. Ultrason.*, vol. 30, pp. 156–163, 1983.

[3] D. Shattuck and O. von Ramm, "Compounding scanning with a phased array," *Ultrason. Imaging*, vol. 4, pp. 93–107, 1982.

[4] G. E. Trahey, S. W. Smith, and O. T. von Ramm, "Speckle pattern correlation with lateral aperture translation: Experimental results and implications for spatial compounding," *IEEE Trans. Ultrason., Ferroelec., Freq. Contr.*, vol. UFFC-33, pp. 257–264, 1986.

[5] J. M. Hansen and J. A. Jensen, "Compounding in synthetic aperture imaging," *IEEE Trans. Ultrason., Ferroelec., Freq. Contr.*, vol. 59, no. 9, pp. 2054–2065, Sept. 2012.

[6] R. F. Wagner, M. F. Insana, and S. W. Smith, "Fundamental correlation lengths of coherent speckle in medical ultrasonic images," *IEEE Trans. Ultrason., Ferroelec., Freq. Contr.*, vol. 35, pp. 34–44, 1988.

[7] M. O'Donnell and S. D. Silverstein, "Optimum displacement for compound image generation in medical ultrasound," *IEEE transactions on ultrasonics, ferroelectrics, and frequency control*, vol. 35, no. 4, pp. 470–476, 1988.

[8] B. Y. S. Yiu, I. K. H. Tsang, and A. C. H. Yu, "Real-time GPU-based software beamformer designed for advanced imaging methods research," in *Proc. IEEE Ultrason. Symp.*, 2010, pp. 1920–1923.

[9] J. M. Hansen, D. Schaa, and J. A. Jensen, "Synthetic aperture beamformation using the GPU," in *Proc. IEEE Ultrason. Symp.*, 2011, pp. 373–376.

[10] M. B. Stuart and J. A. Jensen, "An Architecture and Implementation of Real-time Synthetic Aperture Compounding with SARUS," in *Proc. IEEE Ultrason. Symp.*, Oct. 2011, pp. 1044–1047.

[11] M. Karaman, P. C. Li, and M. O'Donnell, "Synthetic aperture imaging for small scale systems," *IEEE Trans. Ultrason., Ferroelec., Freq. Contr.*, vol. 42, pp. 429–442, 1995.

[12] G. R. Lockwood, J. R. Talman, and S. S. Brunke, "Real-time 3-D ultrasound imaging using sparse synthetic aperture beamforming," *IEEE Trans. Ultrason., Ferroelec., Freq. Contr.*, vol. 45, pp. 980–988, 1998.

[13] C. R. Hazard and G. R. Lockwood, "Theoretical assessment of a synthetic aperture beamformer for real-time 3-D imaging," *IEEE Trans. Ultrason., Ferroelec., Freq. Contr.*, vol. 46, pp. 972–980, 1999.

[14] J. S. Hwang and T. K. Song, "A study of the display pixel-based focusing method in ultrasound imaging," *Ultrason. Imaging*, vol. 23, pp. 1–18, 2001.

[15] S. W. Smith, R. F. Wagner, J. M. Sandrik, and H. Lopez, "Low contrast detectability and contrast/detail analysis in medical ultrasound," *IEEE Trans. Son. Ultrason.*, vol. 30, pp. 164–173, 1983.

[16] J. W. Goodman, "Statistical properties of laser speckle patterns," *Stanford Electron. Lab. Tech. Rep.*, no. 2303-1, 1963.

[17] J. A. Jensen, M. Hansen, B. G. Tomov, S. I. Nikolov, and H. Holten-Lund, "System architecture of an experimental synthetic aperture real time ultrasound system," in *Proc. IEEE Ultrason. Symp.*, Oct. 2007, pp. 636–640.